Proceedings of the 9th World Congress on Momentum, Heat and Mass Transfer (MHMT 2024)
London, United Kingdom – April 11 – 13, 2024
Paper No. ICMFHT 151
DOI: 10.11159/icmfht24.151

Adaptive Mesh Refinement for LES-DEM Study on Heat and Mass Transfer in a Particle-laden Transcritical Jet Flow

Haozhe Su, Hui Jin, Liejin Guo
State Key Laboratory of Multiphase Flow in Power Engineering, Xi'an Jiaotong University
28 Xianning West Road, Xi'an, Shaanxi, China
suhaozhe@stu.xjtu.edu.cn; jinhui@mail.xjtu.edu.cn; lj-guo@mail.xjtu.edu.cn

Abstract – During the feeding process of supercritical water fluidized bed reactors, the particle-laden jet undergoes a transcritical condition upon entering the container, leading to complex and highly coupled flows. To reduce computing resources, we propose an adaptive mesh refinement (AMR) strategy for particle-laden transcritical jets, that is characterized by temperature and velocity fields. When applied to an LES-DEM study, the cell count required is significantly reduced while maintaining a satisfactory accuracy, minimizing the required computational resources and facilitating further study for large-scale reactors. The results indicate the presence of a thermal-shield interface between the jet and the ambient fluid, which dissipates rapidly upon exceeding the critical temperature. Increased particle transportation across this thermal-shield into the ambient fluid notably enhances particle heating efficiency. As the jet injection velocity increases, the Kelvin-Helmholtz instability gradually strengthens interfacial waves, leading to an enhanced stirring up of particles from the primary jet flow, thereby intensifying particle heating. However, the increased jet velocity introduces more low-temperature water and particles, causing a decrease in the overall temperature and an unfavorable condition for efficient particle heating. The compensatory interaction of these factors results in an injection velocity that optimizes efficient particle heating.

Keywords**:** Adaptive mesh refinement, LES-DEM, Transcritical jet, Particle heating, Interfacial instability

1. Introduction

Supercritical water fluidized bed reactors (SCWFBRs) stand out as a promising technology for large-scale hydrogen production due to their reduced susceptibility to plugging [1]. These devices can convert coal or biomass into hydrogen-rich gas efficiently and cleanly. To meet the demands of massive production, SCWFBRs need to be further scaled up and instant respond to operation control, thus efficient numerical simulation becomes an effective way to assist in the scale-up design. However, the nonlinear properties of supercritical water and the considerable particle count pose a significant challenge, the substantial computational resources needed become a bottleneck for simulating large-scale fluidized bed reactors [2]. One solution to this challenge is adaptive mesh refinement (AMR) [3], which selectively enhances mesh resolution in specific regions while economizing resources in less critical areas. Basile *et al*. [4] proposed an *a posteriori* error estimator based on measured energy and jumps at the element interfaces. When applied to a turbulent jet 3D RANS simulation, only 14.7% of the degrees of freedom were needed to closely agree with a classical structured mesh scheme. Cant *et al*. [5] defined a set of refinement criteria based on the flow solution and tested it on several cases of reacting flow. The results indicate that such method may be used for large-scale simulations. The AMR schemes mentioned above are effective in areas such as aerodynamics and reactive flows. However, limitations still exist in studies involving drastic physical property changes in supercritical fluids and nonlinear interactions in particle-laden flows.

During the supercritical water gasification, the feedstock is introduced into the SCWBFR through a nozzle and rapidly heated up in a supercritical environment. Simultaneously, pre-heated water is introduced into the container from its base to maintain a fluidized state. To prevent the formation of undesirable by-products and coking, it is necessary for the feedstock to rapidly heat up and exceed the critical temperature upon entering the reactor. Achieving this necessitates a comprehensive understanding of the intricate transcritical particle-laden flow. In light of this fact, it is necessary to develop an AMR scheme for particle-laden transcritical fluids.

In this study, we propose a solution-based AMR criterion for particle-laden transcritical jets and a corresponding implementation strategy that balances accuracy and efficiency. This proposed criterion is employed in a coupled LES-DEM study to examine the evolution of a transcritical particle-laden jet. Heat transfer characteristics of particles across various

injection velocities are investigated, the dispersion behaviour of particle-laden jets is explored, the stability analysis of the jet is conducted, and finally, the intrinsic mechanism that affects particle heating efficiency is verified.

2. Governing equations

The coupled LES-DEM utilizes the Lagrangian method to track each particle individually, while employing the Eulerian method to treat the fluid as a continuous phase. Assuming a single-phase flow through a porous medium and assigning source terms in governing equations, the particle-fluid interaction is described. The mass, momentum, and energy conservation of fluid is written as:

$$\frac{\partial(\alpha\rho_f)}{\partial t}+\nabla\cdot\left(\alpha\rho_f\mathbf{u}\right)=0, \tag{1}$$

$$\frac{\partial(\alpha\rho_f\mathbf{u})}{\partial t}+\nabla\cdot\left(\alpha\rho_f\mathbf{u}\mathbf{u}\right)=-\alpha\nabla p+\nabla\cdot\left[\alpha(\mathbf{T}_f+\mathbf{T}_{sgs})\right]+\alpha\rho_f\mathbf{g}+\mathbf{F}_p, \tag{2}$$

$$\frac{\partial(\alpha\rho_f C_pT)}{\partial t}+\nabla\cdot(\alpha\rho_f\mathbf{u}C_pT)=\nabla\cdot(\lambda_f C_p\nabla T)+\mathbf{Q}_p. \tag{3}$$

Where α, ρ_f, $\mathbf{u}$, $\mathbf{T}_f$, C_p, T, λ_f are porosity, density, velocity, stress tensor, specific heat, temperature, and thermal conductivity, respectively, the subscript f denotes the fluid. $\mathbf{F}_p$ and $\mathbf{Q}_p$ are the source terms representing momentum and energy transfer between particles and fluids. $\mathbf{T}_{sgs}$ is the sub-grid scale stress tensor solved by Wall-Modeled LES Model (WMLES).

For simplicity, particles in this study are only considered to be affected by gravity, drag force, and contact force on the particles. Heat transfer is limited to convective heat transfer with the fluid and contact heat transfer between particles. Thus, governing equations are expressed as:

$$m_i\frac{d\mathbf{v}_i}{dt}=m_i\mathbf{g}+\mathbf{F}_{d,i}+\sum_{j=1}^{n}\mathbf{F}_{c,ij}, \tag{4}$$

$$m_iC_{p,i}\frac{dT_i}{dt}=\sum_{j=1}^{n}\mathbf{Q}_{c,ij}+\mathbf{Q}_{f,i}. \tag{5}$$

Where m_i, $\mathbf{v}_i$, $C_{p,i}$, T_i are the mass, velocity, specific heat, and temperature of particle i, $\mathbf{F}_{d,i}$ and $\mathbf{Q}_{f,i}$ are the drag force and fluid-particle convection acting on the particle i, $\mathbf{F}_{c,ij}$ and $\mathbf{Q}_{c,ij}$ are the contact force and heat flux between contacted particles i and j.

The calculation of particle drag force $\mathbf{F}_{d,i}$ involves the correlation introduced by Gidaspow [6]. The contact force $\mathbf{F}_{c,ij}$ is delineated through the Hertz-Mindlin contact model, which addresses the normal force component according to the Hertz contact theory [7], and the tangential force component based on the work of Mindlin-Deresiewicz [8, 9]. The convection of fluid-particle interaction $\mathbf{Q}_{f,i}$ is described by the correlation proposed by Ranz and Marshall [10], whereas heat transfer during particle contact $\mathbf{Q}_{c,ij}$ is explicated by the framework of Batchelor and O'brien [11].

3. Numerical simulation

We consider a transcritical jet laden with particles that issues from a feedstock nozzle installed horizontally and is injected into a cylindrical container, as shown in Fig. 1. The cylinder is 400 mm in length and 100 mm in diameter and filled with supercritical water at a pressure of 25 MPa and a temperature of 973 K, with pre-heated water at the same temperature streams in from the bottom. The feedstock nozzle is situated at y=250 mm, with the injected jet kept at a constant temperature of 293 K. Five injection velocities are examined in this study in a range of 0.4 – 0.8 m/s and an interval of 0.1 m/s. This configuration was designed to simulate the feedstock nozzle of a supercritical water fluidized bed reactor [12]. Since the feedstock needs to be heated up rapidly after being injected into the reactor to avoid by-products and coking, it is necessary to study the transcritical processes of room temperature water injection into a supercritical environment as well as the heat and mass transfer characteristics of the particle-laden jet.

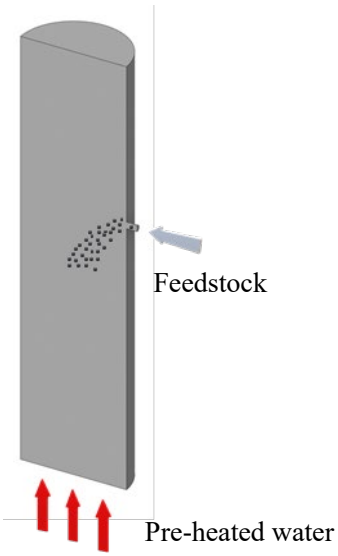

Fig. 1: Cross-section of the computational domain, the cold particle-laden jet is injected from a horizontally installed feedstock nozzle.

To simulate the feeding process of coal slurry in a supercritical water fluidized bed, we consider the particle diameter to be 0.1 mm, the density to be 1400 kg/m^3, the specific heat to be 1680 J/(kg·K) and the particle concentrations to be 3.5wt% in all cases. The particles are randomly generated on the surface where the feedstock enters and have the same initial velocity and temperature as the jet. To achieve adequate fluidization, the pre-heated water flow rate is determined using published experimental data [12, 13]. Additional parameters are listed in Table 1.

Table 1: Physical and simulation parameters of particle and fluid

Term	Value	Term	Value
Particle phase		Fluid phase	
Density	1400 kg/m^3	Pressure	25 MPa
Diameter	0.1 mm	Temperature	973 K
Specific heat	1680 J/(kg·K)	Reference density	60.10 kg/m^3
Thermal conductivity	0.15 W/(m·K)	Viscosity	3.83×10^{-5} Pa·s
Young's modulus	9.9×10^{8} Pa	Specific heat	2726 J/(kg·K)
Restitution coefficient	0.9	Thermal conductivity	0.1146 W/(m·K)
Friction coefficient	0.3	Particle phase time step	1.8×10^{-8} s
		Fluid phase time step	1×10^{-3} s

3.1. Adaptive mesh refinement

With the scale-up of SCWFBRs, the substantial computational resources demanded for numerical simulations pose a significant challenge in the design process. To address this, adaptive mesh refinement (AMR) provides a way to economize resources in less critical areas by selectively enhance mesh resolution in specific regions. For an AMR scheme, the foremost step is to mark cells to be refined according to a preset criterion, which in study is solution-based and as follows:

$$C_{pre-refine} = \left[(y-250\text{mm})^2 + z^2 < (5D)^2\right] \wedge \left\{x \in [0\text{mm}, 300\text{mm}]\right\} \wedge (t < 0.01\text{s}), \tag{6}$$

$$C_{refine} = \left\{\left\{T \in [642.3\text{K}, 652.3\text{K}]\right\} \vee \left[\nabla T > \sigma_{\nabla T}(0.5)\right] \vee \left[\nabla \mathbf{u} > \sigma_{\nabla \mathbf{u}}(0.5)\right] \vee \left[\mathbf{u} > 0.8\max(\mathbf{u})\right]\right\} \wedge (t \geq 0.01\text{s}), \tag{7}$$

$$C_{coarsen} = \left\{T \notin [642.3\text{K}, 652.3\text{K}]\right\} \wedge \left[\nabla T < \sigma_{\nabla T}(0.5)\right] \wedge \left[\nabla \mathbf{u} < \sigma_{\nabla \mathbf{u}}(0.5)\right] \wedge \left[\mathbf{u} < 0.8\max(\mathbf{u})\right]\Big|_{childcells}. \tag{8}$$

Where $\sigma_{\nabla T}(0.5) = \nabla \overline{T} + 0.5 \times \sigma(\nabla T)$ is the average added a factor multiplied by the standard deviation of the variable gradient, D=4 mm is the diameter of feedstock nozzle. The above criteria encompass regions with temperature around the critical temperature (647.3 K) where physical properties change substantially, $\sigma_x(0.5)$ is selected to characterize considerable

gradients in both temperature and velocity fields which fine mesh is required to capture flow details, and 0.8max(**u**) is selected to characterize areas with high-velocity flows within the main jet stream to maintain a reasonable CFL condition. It is noteworthy that the criterion is gradient-dependent, a pre-refined cylindrical region is needed before the computation starts since initial conditions that do not contain gradients, avoiding undesirable results during the first AMR intervals, as Eq. (6) shows.

Once the cells to be refined are determined, the refinement is performed using the PUMA method. In such method, a cell can either be split into multiple child cells or be reclaimed if all its child cells are marked for coarsening, but a cell cannot be further coarsened beyond the original one. Therefore, our strategy is to introduce an initially coarsen mesh, perform an evaluation based on the criterion every 10 time-steps, and refine those cells accordingly. To avoid infinite refinement, we also define a maximum refinement level of 2 and a minimum cell volume of 1.1×10^{-9} m^3, any cell that beyond the limit will not be considered for refinement. The cross-section of mesh during the computation is shown in Fig. 2.

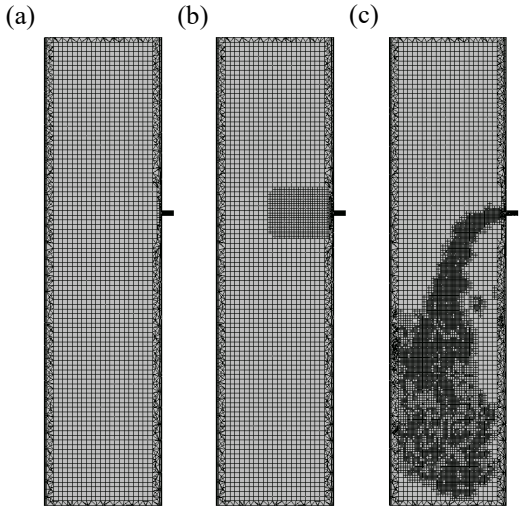

Fig. 2: Cross-section sketch of (a) initial coarsen mesh, (b) pre-refined mesh, and (c) refined mesh during calculation by AMR criteria.

3.2. Validation

To ensure accuracy and efficiency of our mesh adaptation, we conducted a study that compared three different mesh adaptation strategies to a published particle-free transcritical jet case [14]. The validation process employed the same geometry as the original study, which included a cylinder sized 60 mm in diameter and 250 mm in length. The cylinder was fitted with a 5 mm diameter nozzle at the top, where a beam of jet was injected vertically. The jet has a temperature of 370 ℃ and a velocity of 0.05 m/s. The cylindrical container was operated in a supercritical environment with a temperature of 550 ℃ and a pressure of 23 MPa. A cell count of 1.03×10^6 is needed to capture the jet's physical characteristics in the original study, in this study, we prepare two different initial meshes for further adaptation, which have 8.1×10^4 and 1.3×10^5 cells, respectively. As per the criterion, we define three mesh adaptation strategies S_1, S_2, and S_3 as shown in Table 2.

Table 2: Mesh and refinement details in three mesh adaptation strategies.

Strategies	Initial cell count	Hexahedron cell length	Max refinement levels
S_1	1.3×10^5	4 mm	2
S_2	1.3×10^5	4 mm	1
S_3	8.1×10^4	5 mm	2

Given the initial mesh and adaptation strategies, the validation of the simulation can be carried out by comparing the time-mean axial velocity at the central axis, as shown in Fig. 3.

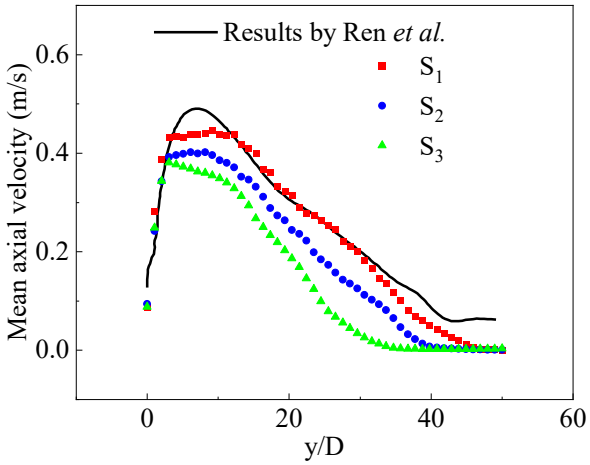

Fig. 3: Comparison of mean axial velocity among three mesh adaptation strategies in this work and results reported by Ren *et al*.[14]

The above comparison shows that the S_1 strategy is consistent with the findings of Ren *et al*. [14], except for a minor variation in maximum speed. Conversely, the S_2 and S_3 strategies display slight differences caused by inadequate computational resolution due to the initial coarsen mesh and insufficient refinement levels. Therefore, we will implement the S_1 strategy with an initial mesh of comparable size in our study. Compared with a uniformly fine mesh scheme with 8.30×10^6 cells, the implement of such AMR scheme could significantly reduce cell count required by 86.6%, while maintaining an average error of 5.60% in velocity and 0.09% in temperature. In the context of this significant reduction in computing resources, a study of jet flow in SCWFBR with considerable particles can be conducted.

4. Results and discussion

When particles and the jet are injected from the feedstock nozzle, they rapidly disperse and heat up by the ambient fluid, as shown in Fig. 4. At low injection velocities, particles lose horizontal velocity upon entering the reactor and descend along the wall. As the jet velocity increases, the jet takes on a more parabolic shape and impacts the opposite wall at high injection velocities. Once the jet reaches its critical temperature, a layer of fluid with high specific heat can be found. Here, the fluid absorbs heat primarily to reduce its density rather than increase its temperature, forming a thermal-shield layer with significant density stratification on both sides. Due to the thermal-shield layer, most particles are heated to the critical temperature but are difficult to exceed it. Only a small number of particles located near the jet interface are stirred into the ambient fluid, thus, to be rapidly heated.

The cross-sectional analysis was conducted to examine the temperature distribution of particles within a jet at an injection velocity of 0.6 m/s at time t=0.55 s, as depicted in Fig. 5 (a). Upon entering the container, the particle-laden jet displays distinct developmental characteristics. Initially, particles are uniformly distributed in a regular cylindrical jet, namely the jet region. Within this region, the particle temperature exhibits clear stratification: the outer ring of particles reaches the critical temperature, while central particles remain at a lower temperature. As the injection progresses, a considerable portion of particles reaches the critical temperature. At the jet interface, due to density stratification near the thermal-shield, distinct Kelvin-Helmholtz instabilities arise, causing particle agitation and their traversal across the thermal-shield into the high-temperature ambient fluid, characterizing the transcritical region. This phenomenon significantly contributes to particle dispersion and enhances heating efficiency. Further heating of the jet leads to the majority of particles exceeding the critical temperature, prompting a swift increment in their temperature. Consequently, the jet's morphology becomes irregular and transition into the dispersion zone, experiencing rapid particle heating.

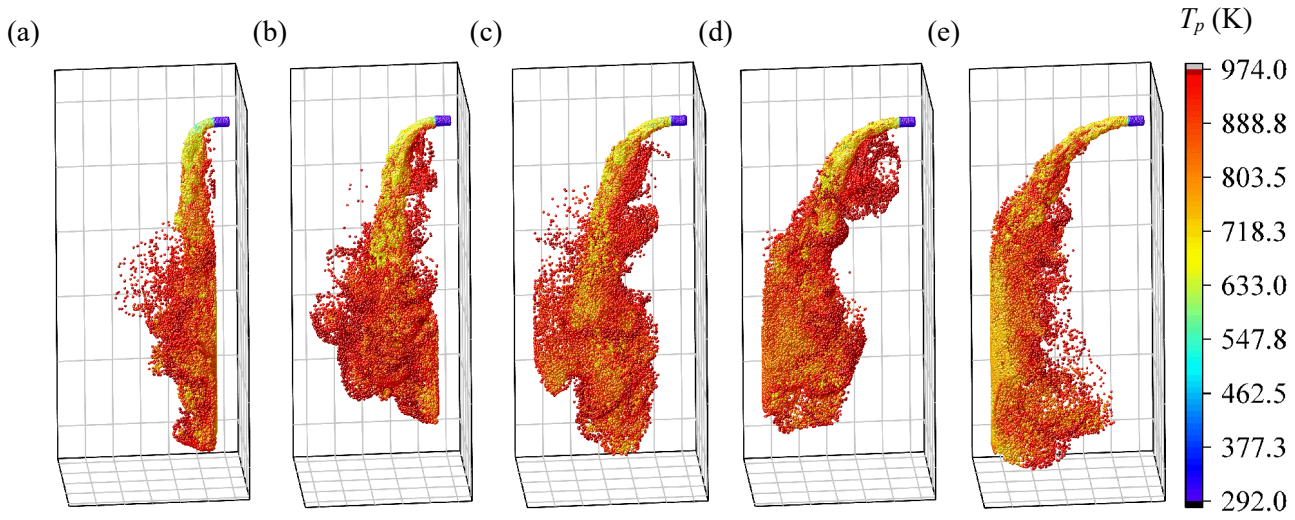

Fig. 4: Particles and their temperature distribution at t=0.55 s, injection velocity ranges from (a) 0.4 m/s to (e) 0.8 m/s in 0.1 m/s increments.

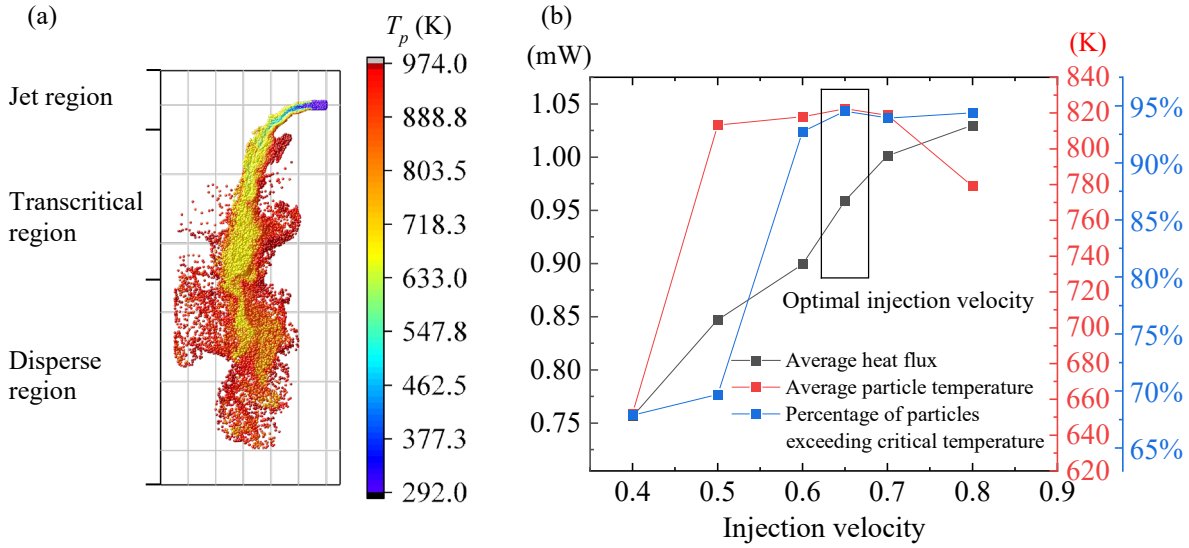

Fig. 5: (a) Jet and particle cross-section partitioning at injection velocity of 0.6 m/s and t=0.55 s, (b) average particles heat transfer characteristics at final moment t=1 s for different injection velocities.

We further examined the average particle temperature, average heat flux between particles and the fluid, and percentage of particles exceeding the critical temperature at final moment, as shown in Fig. 5 (b). Notably, the average particle heat flux increased with increasing injection velocities. However, the average particle temperature and percentage of particles exceeding the critical temperature initially increased and then decreased. Thus, we conducted an additional computation at injection velocity of 0.65 m/s and identified an optimal injection velocity that maximized particle heating efficiency. Compared with two alternative scenarios, a jet descent along the wall at 0.4 m/s and impact against the opposite wall at 0.8 m/s, the average temperature of particles had an increment of 170.3 K and 43.3 K, respectively. However, the advantage in the count of particles exceeding the critical temperature is not substantial, displaying increases of 26.7% and 0.2%, correspondingly.

To reveal the fundamental mechanism behind this optimal velocity, the effect of injection velocity on surface instabilities is investigated. Instead of complex linear or nonlinear stability analysis, we evaluate the intensity of jet instability across various injection velocities by measuring the deviation between the perturbed state, obtained from the instantaneous flow

field through LES, and the unperturbed base state obtained from the time-averaged flow field via RANS. Taking the center cross-section D, the disturbance energy in velocity is defined as:

$$E_d = \iint_D |\mathbf{u} - \mathbf{u}_b| \mathrm{d}x\mathrm{d}y. \tag{9}$$

It should be noted that the 'energy' does not denote physical energy but rather serves as a metric quantifying the level of velocity deviation, representing the intensity of particles stirring from the jet into the ambient fluid. The velocity field snapshots of perturbed and unperturbed states are shown in Fig. 6 (a), the distribution of disturbance energy is illustrated in Fig. 6 (b), and the time evolution of disturbance energy is shown in Fig. 6 (c).

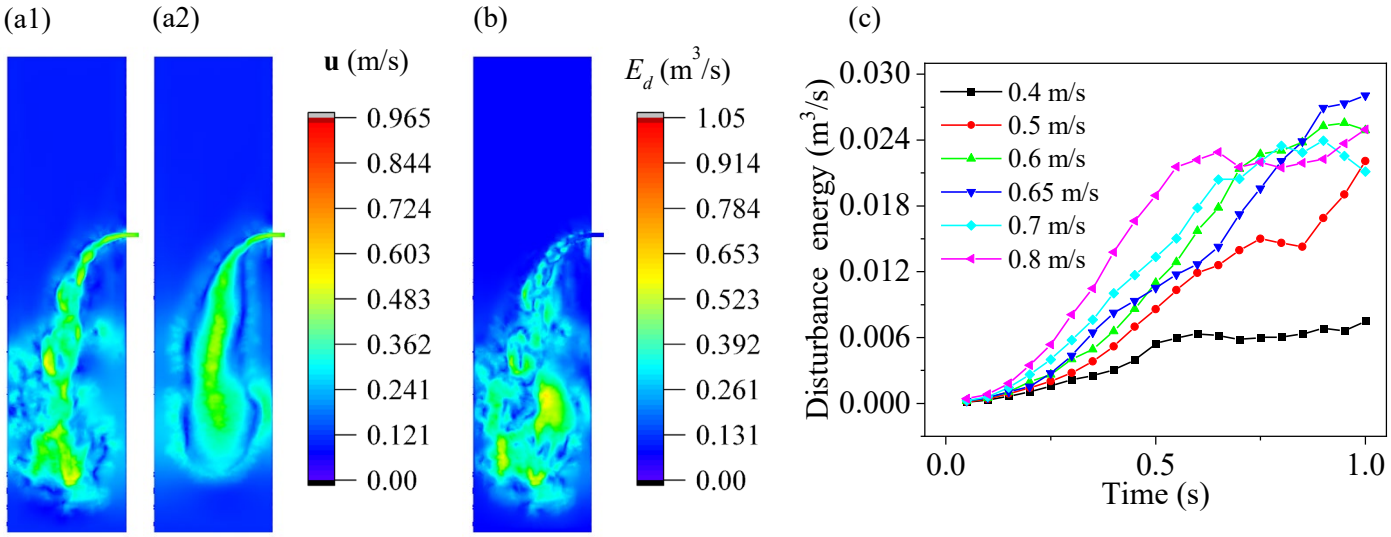

Fig. 6: Snapshot at injection velocity 0.65 m/s and t=0.5s of: (a1) fluid velocity field via LES, (a2) fluid velocity field via RANS, (b) distribution of disturbance energy. (c) Time evolution of disturbance energy among different injection velocities.

The distribution of disturbance energy indicates an infinitesimal energy within the jet, while a notable concentration of energy at the interface where the jet interacts with the ambient fluid. This localized concentration leads to the development of a Kelvin-Helmholtz instability at the jet interface, contributing to the agitation of particles across the thermal-shield into the ambient fluid. Such phenomenon significantly augments both particle dispersion and heating efficiency. Over time, surface instability gradually amplifies, and the disturbance energy increases by 248.2% when the injection velocity varies from 0.4 to 0.8 m/s during the initial 0.5 s. However, at the final moment t=1 s, the disturbance energy corresponding to the maximum injection velocity increases by 233.8%, while the disturbance energy corresponding to the optimal injection velocity increases by 275.1%. Therefore, further increasing the injection velocity contributes less to the enhancement of instabilities. For low-temperature fluids introduced by jets, the resultant enthalpy drop is directly proportional to both time and injection velocity. An increase in injection velocity corresponds to a decrease in the internal temperature of the container, unfavorably impacting particle heating. These two compensatory factors converge at an optimal injection velocity, maximizing particle heating efficiency.

5. Conclusion

A solution-based adaptive mesh refinement (AMR) criterion for particle-laden transcritical jets is proposed, applying it to a coupled LES-DEM study, we investigate the transcritical process of a particle-laden jet. By employing AMR, the cell count required for the computational domain in this study is significantly reduced by about 86.6% compared to a uniformly fine mesh, while maintaining a maximum error of 5.60%. The particle-laden jet disperses and heats up within the supercritical environment. As the jet is heated to the critical temperature, a thermal-shield layer is formed that prevents further heating of the particles. Upon the initially regular-shaped jet entering the container, the jet interface generates instability waves due to the presence of Kelvin-Helmholtz instabilities, which significantly amplify particle dispersion and heating. Higher injection velocities initially increase average particle temperature until peaking at 0.65 m/s, representing optimal particle heating

efficiency. Compared with low and high injection velocities, the average particle temperature exhibited increments of 170.3 K and 43.3 K, correspondingly, and the percentage of particles exceeding the critical temperature increased by 26.7% and 0.2%, respectively. Analysis of disturbance energy reveals concentration at the jet interface, driving Kelvin-Helmholtz instability and intensifying particle heating. During the initial 0.5 s, increasing injection velocity could lead to a disturbance energy increase of 248.2%. At the final moment, however, such an increase does not increase with increasing injection velocity but rather maximizes at 0.65 m/s. On the other hand, an increase in the injection velocity introduces more low-temperature water, reducing the overall temperature of the container and causing an unfavorable condition for particle heating. The above two compensating factors lead to an optimal injection rate that maximizes particle heating efficiency.

Acknowledgements

The authors acknowledge the support of the National Key R&D Program of China (2020YFA0714400).

References

[1] H. Jin, Y. Lu, B. Liao, L. Guo, and X. Zhang, "Hydrogen production by coal gasification in supercritical water with a fluidized bed reactor," *Int. J. Hydrogen Energy,* vol. 35, no. 13, pp. 7151-7160, 2010.

[2] H. Zhang, Y. Wu, X. An, and A. Yu, "Numerical investigation on the scale-up rules of a supercritical water fluidized bed reactor using the two-fluid model," *Eng. Appl. Comput. Fluid Mech.,* vol. 15, no. 1, pp. 1830-1842, 2021.

[3] M. J. Berger and J. Oliger, "Adaptive mesh refinement for hyperbolic partial differential equations," *J. Comput. Phys.,* vol. 53, no. 3, pp. 484-512, 1984.

[4] F. Basile, J.-B. Chapelier, M. de la Llave Plata, R. Laraufie, and P. Frey, "Unstructured h-and hp-adaptive strategies for discontinuous Galerkin methods based on a posteriori error estimation for compressible flows," *Comput. Fluids,* vol. 233, p. 105245, 2022.

[5] R. Cant, U. Ahmed, J. Fang, N. Chakarborty, G. Nivarti, C. Moulinec, and D. Emerson, "An unstructured adaptive mesh refinement approach for computational fluid dynamics of reacting flows," *J. Comput. Phys.,* vol. 468, p. 111480, 2022.

[6] D. Gidaspow, *Multiphase flow and fluidization: continuum and kinetic theory descriptions*. San Diego: Academic press, 1994.

[7] H. Hertz, "Ueber die Berührung fester elastischer Körper," *J. für die Reine und Angew. Math.,* vol. 92, no. 156, 1881.

[8] R. D. Mindlin, "Compliance of elastic bodies in contact," *J. Appl. Mech.,* vol. 16, no. 3, pp. 259-268, 1949.

[9] R. D. Mindlin and H. Deresiewicz, "Elastic spheres in contact under varying oblique forces," *J. Appl. Mech.,* vol. 20, no. 3, pp. 327-344, 1953.

[10] W. E. Ranz and W. R. Marshall, "Evaporation from Drops-I and-II," *Chem. Eng. Progr,* vol. 48, pp. 141-146,173-180, 1952.

[11] G. K. Batchelor and R. O'brien, "Thermal or electrical conduction through a granular material," *Proc. R. Soc. London, Ser. A,* vol. 355, no. 1682, pp. 313-333, 1977.

[12] Y. Lu, H. Jin, L. Guo, X. Zhang, C. Cao, and X. Guo, "Hydrogen production by biomass gasification in supercritical water with a fluidized bed reactor," *Int. J. Hydrogen Energy,* vol. 33, no. 21, pp. 6066-6075, 2008.

[13] H. Jin, C. Fan, L. Guo, S. Liu, C. Cao, and R. Wang, "Experimental study on hydrogen production by lignite gasification in supercritical water fluidized bed reactor using external recycle of liquid residual," *Energy Convers. Manage.,* vol. 145, pp. 214-219, 2017.

[14] Y. Ren, Z. Wu, X. Meng, G. Ou, J. Kou, H. Jin, and L. Guo, "Large eddy simulation of water jets under transcritical and supercritical conditions," *J. Supercrit. Fluids.,* vol. 187, p. 105648, 2022.